



# Combining Electrochemical and Theoretical Analysis to Evaluate Hydrogen Permeation Inhibitors During Free Corrosion

Raquel L. Silvério<sup>a</sup>, Rodrigo G. de Araujo<sup>b</sup>, Thais T. Carvalho<sup>b</sup>, Bhetina C. Gomes<sup>a</sup>,  
Ludmila de O. Borges<sup>b</sup>, Matheus G. Silva<sup>a</sup>, Lilian W. Coelho Paes<sup>c</sup> , Diego P. Sangi<sup>b</sup>,  
Julliane Yoneda<sup>b</sup>, Elivelton A. Ferreira<sup>a,b,\*</sup> 

<sup>a</sup>Universidade Federal Fluminense, Programa de Pós-Graduação em Engenharia Metalúrgica, Volta Redonda, RJ, Brasil.

<sup>b</sup>Universidade Federal Fluminense, Instituto de Ciências Exatas, Volta Redonda, RJ, Brasil.

<sup>c</sup>Escola de Engenharia Industrial e Metalurgia de Volta Redonda, Departamento de Ciências Exatas, Volta Redonda, RJ, Brasil.

Received: April 11, 2023; Revised: September 25, 2023; Accepted: September 25, 2023

In this work, electrochemical tests were performed to measure hydrogen permeation during free dissolution of carbon steel in the presence of the ionic liquids (ILs) 1-ethyl-3-methylimidazolium acetate [(EMIM)<sup>+</sup>(Ac)<sup>-</sup>], 1-ethyl-3-methylimidazolium bromide [(EMIM)<sup>+</sup>(Br)<sup>-</sup>], and 1-butyl-3-methylimidazolium tetrafluoroborate [(BMIM)<sup>+</sup>(BF<sub>4</sub>)<sup>-</sup>] in 5.4 mol L<sup>-1</sup> HCl aqueous solution. The permeation inhibition efficiencies (IEp (%)) of 5-hydroxy-2-nitromethylene-hexahydropyrimidine (HPY) and a commercial corrosion inhibitor (CCI) were also evaluated. Among the ILs, the (BMIM)<sup>+</sup>(BF<sub>4</sub>)<sup>-</sup> compound presented the highest corrosion and hydrogen permeation inhibition efficiencies, with values of 23% and 30%, respectively. The (EMIM)<sup>+</sup>(Br)<sup>-</sup> and (EMIM)<sup>+</sup>(Ac)<sup>-</sup> compounds were not effective against corrosion, but they presented IEp of 15.8% and 23%, respectively. The HPY compound demonstrated 61% effectiveness in preventing corrosion, while *in silico* evaluation indicated no toxicity. However, neither the HPY compound nor the CCI compound inhibited the entry of hydrogen into the carbon steel during the pickling process.

**Keywords:** Carbon steel, hydrogen permeation, Devanathan-Stachurski cell, corrosion, ionic liquids.

## 1. Introduction

Steel structures can suffer from severe damage, such as brittle fracture, due to the absorption of hydrogen atoms<sup>1-3</sup>. Hydrogen can also penetrate the steel crystal lattice or lattice defects during acid cleaning, leading to embrittlement<sup>4-6</sup>. In many industries, hydrochloric or sulfuric acids are used at concentrations up to 20% in pickling processes to remove scale and in oil well acidizing, with organic inhibitors being used to prevent corrosion of steel<sup>1,2,7-10</sup>. However, it is not guaranteed that these inhibitors can also function as hydrogen permeation inhibitors<sup>11-14</sup>. Moreover, there is a lack of systematic experimental studies investigating the effect of organic inhibitors on acid pickling corrosion<sup>11,15,16</sup>, while even fewer studies have addressed hydrogen permeation inhibition<sup>4,6,17</sup>.

Ionic liquids (ILs) are compounds with high ionic conductivity, nonflammability, and high thermal stability<sup>18-20</sup>. Recently, these compounds have been evaluated as steel corrosion inhibitors. For instance, alkylimidazolium-based ILs, such as 1-ethyl-3-methylimidazolium acetate [(EMIM)<sup>+</sup>(Ac)<sup>-</sup>] and 1-butyl-3-methylimidazolium

tetrafluoroborate [(BMIM)<sup>+</sup>(BF<sub>4</sub>)<sup>-</sup>], have demonstrated notable inhibition efficiencies against the corrosion of carbon steel in HCl solution<sup>21-23</sup>. However, these corrosion inhibition studies were conducted using aqueous solutions containing up to 2 mol L<sup>-1</sup> of HCl.

In recent work<sup>6</sup>, the authors used a modified Devanathan-Stachurski (D-S) cell, where loading of hydrogen occurred during freely corroding steel dissolution in a pickling process employing a high concentration of hydrochloric acid (16.5%). In another study<sup>24</sup> the authors designed a device to assess hydrogen permeation into steel during free corrosion in marine environments.

In earlier work<sup>17</sup>, researchers employed the D-S method to analyze the effectiveness of certain ionic liquid (IL) compounds in inhibiting hydrogen permeation in SAE 1020 steel. Specifically, the ILs (BMIM)<sup>+</sup>(BF<sub>4</sub>)<sup>-</sup> and (BMIM)<sup>+</sup>(Cl)<sup>-</sup> were evaluated and demonstrated 59% efficiency in inhibiting hydrogen permeation.

In the present work, in order to better understand the effects of ionic liquids on hydrogen permeation, investigation was made of the imidazolium ionic liquids 1-ethyl-3-methylimidazolium acetate [(EMIM)<sup>+</sup>(Ac)<sup>-</sup>] and 1-ethyl-3-methylimidazolium bromide [(EMIM)<sup>+</sup>(Br)<sup>-</sup>].

\*e-mail: [eliveltonalves@id.uff.br](mailto:eliveltonalves@id.uff.br)

Also tested were the permeation inhibition efficiencies of a new compound synthesized in our laboratory, namely 5-hydroxy-2-nitromethylene-hexahydropyrimidine (HPY), and a commercial corrosion inhibitor (CCI) used in pickling lines in the hot-dip galvanized steel industry.

In addition, quantum chemical calculations have been widely used to study reaction mechanisms and to elucidate many experimental observations. They have proven to be important tools in scientific corrosion research. Advances in methodology and implementation have reached the point where the predictive properties are reasonable and accuracy can be obtained from density functional theory (DFT) calculations<sup>17,25-28</sup>.

The inhibition efficiency is related to molecular and structural parameters. The geometry of the inhibitor in its ground state, as well as the nature of the molecular orbitals, can be obtained by DFT calculation<sup>29,30</sup>. Several quantum parameters are widely used to describe aspects of chemical reactions such as chemical selectivity, reactivity, and charge distribution.

The evaluation of corrosion inhibition properties is carried out by the analysis of HOMO (highest occupied molecular orbital) energy, LUMO (lowest unoccupied molecular orbital) energy, hardness ( $\eta$ ), softness ( $S$ ), global electrophilicity index ( $\omega$ ), the fraction of electrons transferred ( $\Delta N$ ), and electronegativity ( $\chi$ ).

Finally, considering the damage caused to the environment and ecosystems by most of the inhibitors in current use, *in silico* evaluation of HPY toxicity was performed.

## 2. Materials and Methods

### 2.1. Materials

The working electrodes were steel sheets with dimensions of 2.5 x 2.5 x 0.2 cm. The composition, ferrite/pearlite phases, grain size, and hardness (Table 1) were determined according to ASTM E 415<sup>a</sup>, ABNT NBR ISO 6508 - 1 and 2<sup>b</sup>, and ASTM E 45<sup>c</sup>.

For the analyses, the surfaces of the SAE 1008 and SAE 1020 carbon steels were polished with different grade emery papers (200, 400, 600, 800, and 1200), followed by rinsing with deionized (Milli-Q) water. Carbon steel obtained after the hot strip mill process was also studied in this work. The nominal composition of this steel is shown in Table 1. For each steel sample, a geometrical area of 1 cm<sup>2</sup>, delimited by an O-ring, was exposed to the electrolytes.

The compounds (EMIM)<sup>+</sup>(Ac)<sup>-</sup>, (EMIM)<sup>+</sup>(Br)<sup>-</sup>, and (BMIM)<sup>+</sup>(BF<sub>4</sub>)<sup>-</sup> (Figure 1a), with purity  $\geq 95\%$ , acids, and cleaning materials used in the experiments were acquired from Merck Sigma-Aldrich. The HPY inhibitor was produced in the laboratory (Figure 1b), according to the modified synthesis described previously<sup>31</sup>, using a mixture of 1,3-diaminepropan-2-ol (5 mmol) and 1,1-bis-methylsulfanyl-2-nitromethylene (5 mmol), with ethanol (15 mL) as solvent, in a flask suitable for reactions in a microwave reactor (reaction 1). Microwave irradiation was applied for 20 min, to assist the double vinylic substitution according to an addition-elimination mechanism, producing 5-hydroxy-2-nitromethylenehexahydropyrimidine (HPY), with a yield of 82% after purification by filtration and extensive washing using cold ethanol.

**Table 1.** Chemical composition, phases, hardness, and grain size of the carbon steels.

Carbon steel	Composition (wt.%) <sup>a</sup>				Rockwell hardness (HRB) <sup>b</sup>	Grain size ( $\mu\text{m}$ ) <sup>c</sup>	Pearlite (%) <sup>c</sup>	Phase distribution <sup>c</sup>
	C	Mn	P	S				
SAE 1008	0.08	0.27	0.02	0.01	82.9	9.5	4.5	random
SAE 1020	0.18	0.53	0.02	0.01	61.6	*	48.2	random
Steel with scale	0.06	0.35	0.02	0.02	65.1	8.5	4.4	random

\*It was not possible to determine the grain size of the 1020 sample, because the microstructure matrix was 48.2% pearlite.

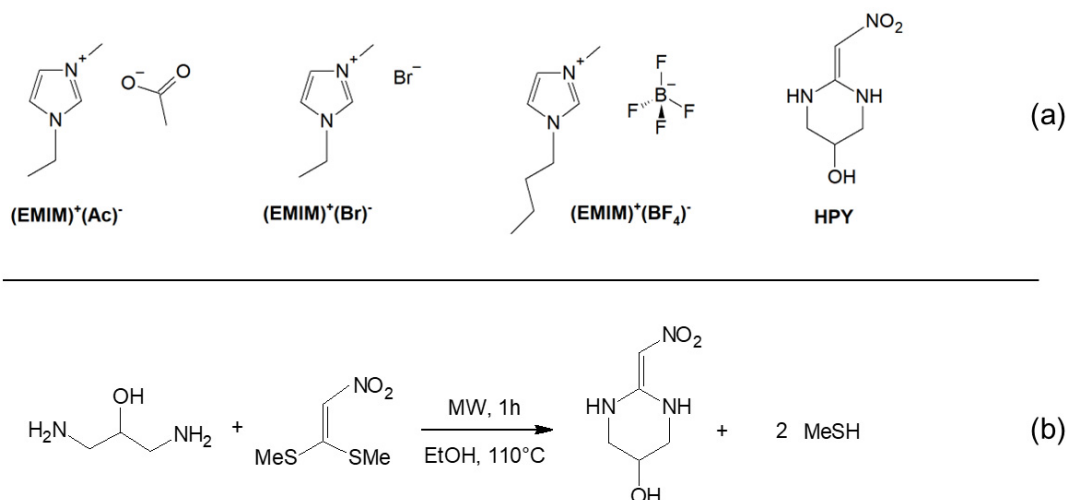


**Figure 1.** Structures of the compounds (EMIM)<sup>+</sup>(Ac)<sup>-</sup>, (EMIM)<sup>+</sup>(Br)<sup>-</sup>, (BMIM)<sup>+</sup>(BF<sub>4</sub>)<sup>-</sup>, and HPY. (a), and synthesis reaction of HPY compound (b).

The NMR chemical shifts of the HPY compound are given below:

$^1\text{H}$  NMR (DMSO- $d_6$ ):  $\delta$  8.90-8.74 (m, 2H), 6.28 (s, 1H), 5.31 (d,  $J = 2.5$  Hz, 1H), 4.06-3.98 (m, 1H), 3.39-3.32 (m, 2H), 3.20-3.10 (m, 2H).

$^{13}\text{C}$  NMR (DMSO- $d_6$ ):  $\delta$  154.23, 98.47, 58.38, 44.57.

Aqueous solutions containing 5.4 and 2.7 mol L $^{-1}$  of the acids HCl and H $_2$ SO $_4$ , respectively, were prepared using deionized (Milli-Q) water.

Solutions containing 2 mmol L $^{-1}$  of (EMIM) $^+$ (Ac) $^-$ , (EMIM) $^+$ (Br) $^-$ , and HPY, and 1.1 mmol L $^{-1}$  of (BMIM) $^+$ (BF $_4$ ) $^-$ , were prepared in the HCl solution. A solution containing 0.02 mL L $^{-1}$  of the commercial corrosion inhibitor (CCI) was also evaluated. This inhibitor is used in pickling lines in the hot-dip galvanized steel industry.

The steels exposed to the different inhibitors and electrolytes are summarized in Table 2.

## 2.2. Electrochemical measurements

The experiment involved the acquisition of hydrogen permeation transients, polarization curves (PC), and electrochemical impedance spectroscopy (EIS) data, using a potentiostat (Sensit BT, PalmSens). The counter and reference electrodes used were Pt and Ag|AgCl|KCl $_{\text{sat}}$ , respectively.

Hydrogen permeation during free corrosion of the steels in HCl and H $_2$ SO $_4$  solutions was determined in the presence and absence of inhibitors, using a D-S type cell $^{6,32}$  (Figure 2).

The detection side employed 0.2 mol L $^{-1}$  NaOH solution, which is a commonly used alkaline solution $^6$ . On this side, atomic hydrogen was performed by anodizing the steel at 0.0 V (vs. Ag|AgCl|KCl $_{\text{sat}}$ ). At this potential, the anodic current density was very low, due to formation of the passive oxide film. Therefore, the recorded current could be attributed exclusively to the atomic hydrogen formed on the hydrogen generation side of the sample.

The polarization curves (PCs) were obtained in the cathodic region, with scanning from -150 to +150 mV vs. OCP, at a rate of 0.166 mV s $^{-1}$ .

The EIS measurements were performed by applying an AC potential of 10 mV (rms) on the corresponding DC potential value of 0.0 V (vs. Ag|AgCl|KCl $_{\text{sat}}$ ) on the hydrogen detection side. At this potential, the steel was passivated, allowing for a correlation between the current density and the atomic hydrogen formed on the hydrogen generation side of the sample $^6$ . The experiments were conducted in the frequency range from 10.0 kHz to 10 mHz, with acquisition of 10 points per frequency decade. Z-view $^{\text{®}}$  software was used to fit the equivalent electrical circuits (EECs) to the experimental data. To account for non-ideal capacitive responses, capacitance was used to replace the constant phase elements (CPEs) in the EECs.

## 2.3. Weight loss measurements

The corrosion resistance of the steel was determined using the gravimetric method, which involved weighing the steel before and after pickling in aqueous acid solutions

**Table 2.** Steels exposed to the different inhibitors and electrolytes.

Solutions	Steels
2.7 mol L $^{-1}$ H $_2$ SO $_4$ aqueous solution	1020
5.4 mol L $^{-1}$ HCl aqueous solution	1008, 1020, and carbon steel (obtained after the hot strip mill process)
5.4 mol L $^{-1}$ HCl aqueous solution + 2 mmol L $^{-1}$ of (EMIM) $^+$ (Ac) $^-$	1020
5.4 mol L $^{-1}$ HCl aqueous solution + 2 mmol L $^{-1}$ of (EMIM) $^+$ (Br) $^-$	1020
5.4 mol L $^{-1}$ HCl aqueous solution + 2 mmol L $^{-1}$ of HPY	1020
5.4 mol L $^{-1}$ HCl aqueous solution + 1.1 mmol L $^{-1}$ of (BMIM) $^+$ (BF $_4$ ) $^-$	1008
5.4 mol L $^{-1}$ HCl aqueous solution + 2 mmol L $^{-1}$ of CCI	carbon steel (obtained after the hot strip mill process)

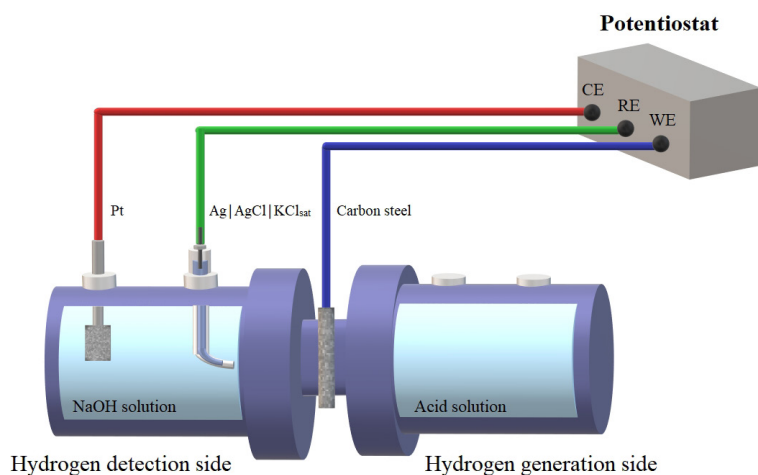


**Figure 2.** Schematic illustration of the Devanathan-Stachurski type cell.

in the D-S cell. The difference in weight was then used to estimate the efficiency of the corrosion resistance.

## 2.4. Computational details

Complete geometrical optimizations of the investigated compounds were performed using density functional theory (DFT), employing the Becke three-parameter hybrid functional and the Lee-Yang-Parr correlation functional (B3LYP)<sup>33,34</sup>, with the 6-311G(d,p) basis set, performed using Gaussian 09 software<sup>35</sup>. Vibrational analyses of the optimized structures determined whether they corresponded to a maximum or a minimum in the potential energy curve, with no imaginary frequencies being found.

The reactivity descriptors including electronegativity ( $\chi$ ), hardness ( $\eta$ ), softness (S), and the fraction of electrons transferred ( $\Delta N$ ) were calculated from the energies of the highest occupied molecular orbital (HOMO) and the lowest unoccupied molecular orbital (LUMO)<sup>36</sup>.

These descriptors were obtained using Koopmans' theorem, where  $E_{\text{HOMO}}$  and  $E_{\text{LUMO}}$  of the inhibitor molecule were related to the ionization potential (I) and the electron affinity (A)<sup>37</sup>:

$$I = -E_{\text{HOMO}} \text{ and } A = -E_{\text{LUMO}} \quad (1)$$

$$\chi = \frac{I + A}{2} \quad (2)$$

$$\eta = \frac{I - A}{2} = -\frac{E_{\text{LUMO}} - E_{\text{HOMO}}}{2} \quad (3)$$

$$S = \frac{1}{\eta} \quad (4)$$

$$\Delta N = \frac{\chi_{\text{Fe}} - \chi_{\text{inh}}}{2\eta_{\text{inh}}} \quad (5)$$

where,  $\chi_{\text{Fe}}$  and  $\eta_{\text{Fe}}$  are the electronegativity and hardness of iron, respectively.

## 2.5. In silico toxicity predictions

HPY toxicity was predicted using the freely available models Toxicity Estimation Software Tool (T.E.S.T.)<sup>38</sup> and Toxtree<sup>39</sup>.

Based on 2D molecular descriptors, T.E.S.T. can predict toxicity values for different test models<sup>38</sup>. The software is available online, providing predictions of toxicity based on quantitative structure-activity relationship (QSAR) mathematical models.

Toxtree applies a decision tree approach to estimate toxic hazard<sup>39</sup>. Benigni/Bossa rules for carcinogenicity and mutagenicity were used to obtain the predictions<sup>40</sup>.

## 3. Results and Discussion

### 3.1. Electrochemical measurements

#### 3.1.1. Hydrogen generation side

Figure 3 presents the polarization curves for the SAE 1020 steel in aqueous HCl and H<sub>2</sub>SO<sub>4</sub> solutions. It can be seen that the current densities in the cathodic branch for steel immersed in HCl solution were slightly higher than

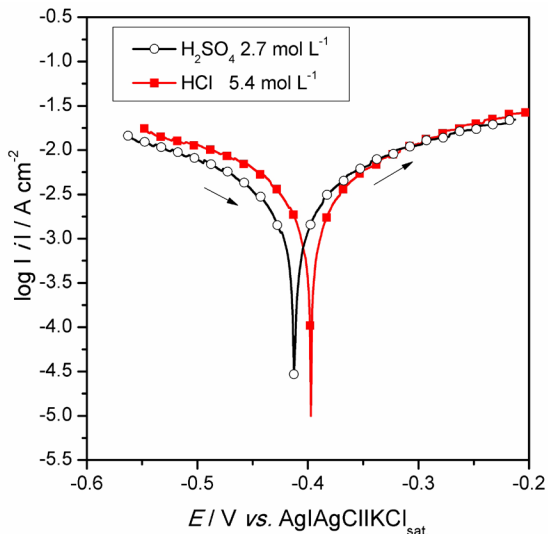
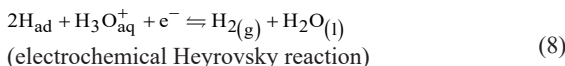


**Figure 3.** Polarization curves for the SAE 1020 steel in aqueous HCl and H<sub>2</sub>SO<sub>4</sub> solutions.

obtained in H<sub>2</sub>SO<sub>4</sub> solution. On the other hand, the current densities in the anodic branch were similar for steel immersed in both solutions.

The following electrochemical and chemical reactions (6-8) occur at the cathodic sites<sup>41</sup>:



At the anodic sites, dissolution of the metal occurs (9):



The steel immersed in HCl solution also presented a slightly higher OCP value. The lower H<sub>2</sub>SO<sub>4</sub> concentration, compared to the HCl solution, and the low degree of ionization to HSO<sub>4</sub><sup>-</sup> in the solution decreased hydrogen reduction in the cathodic branch.

Although a small difference in electrochemical behavior was observed for the steel immersed in the two solutions, the mass losses determined by the gravimetric method were equal. The mass loss value after 4.5 h of immersion in acid solution was (73 ± 11) mg cm<sup>-2</sup>.

#### 3.1.2. Hydrogen detection side

Figure 4 shows the hydrogen permeation transients (ip) for the SAE 1020 steel during pickling in aqueous HCl and H<sub>2</sub>SO<sub>4</sub> solutions. The hydrogen permeation results for measurements carried out in HCl and H<sub>2</sub>SO<sub>4</sub> solutions were used to define the base electrolyte for the subsequent tests utilizing inhibitors.

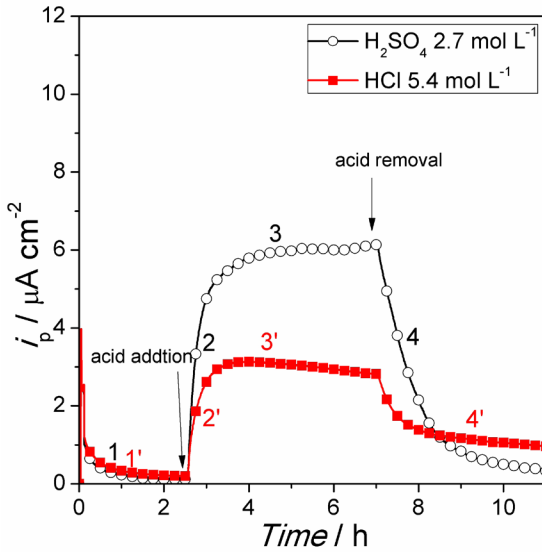


**Figure 4.** Hydrogen permeation transients for the SAE 1020 steel during pickling in aqueous HCl and H<sub>2</sub>SO<sub>4</sub> solutions.

The detection of atomic hydrogen was performed by anodizing the steel at 0.0 V (vs. Ag|AgCl|KCl<sub>sat</sub>). Due to formation of the passive oxide film, the recorded current could be attributed exclusively to the atomic hydrogen formed on the hydrogen generation side of the sample.

The corrosion process on the hydrogen generation side resulted in the production of adsorbed (ad) hydrogen atoms. These atoms could then be absorbed (ab) by the steel:



The hydrogen permeation transients (Figure 1) presented three distinct regions with differing behaviors. Regions 1 and 1' were recorded up to 2.5 h, before acid addition on the hydrogen generation side. These current densities corresponded to the transportation of vacancies across the passive film. In region 2, which began at 2.5 h, acid solutions were introduced to the hydrogen generation side. Within approximately 4 min, the current density increased until reaching the steady-state permeation current, denoted as  $i_p^{ss}$ . The transient process lasted approximately 1 h, during which time regions 3 and 3' were observed. The current densities for the steel samples immersed in H<sub>2</sub>SO<sub>4</sub> and HCl solutions were approximately 6 and 3  $\mu\text{A cm}^{-2}$ , respectively, in these regions.

Previous work investigated the effects of chloride ions on the kinetics of the hydrogen evolution reaction and on hydrogen absorption and permeation at an iron surface in 0.5 mol L<sup>-1</sup> H<sub>2</sub>SO<sub>4</sub> solution, at 23 °C, using the D-S permeation method<sup>43</sup>. According to the authors, a decrease in hydrogen permeation could be attributed to an increase in the rate constant of the H<sub>2</sub> formation step (reaction 7) and/or a shift of the equilibrium position towards the adsorption side (reaction 10).

These results were consistent with the polarization curves (Figure 3), which showed that the presence of chloride acted to increase the current densities in the cathodic branch, and were also in agreement with previous work<sup>43</sup>.

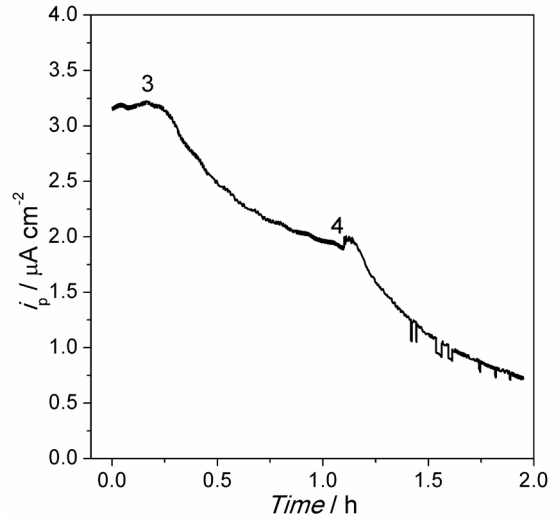


**Figure 5.** Hydrogen permeation transient measurements, on the hydrogen detection side, for the SAE 1020 steel after removal of the HCl solution.

In order to ensure that the current density was associated with hydrogen permeation, the H<sub>2</sub>SO<sub>4</sub> and HCl solutions were removed from the hydrogen generation side. After this, the current densities decreased exponentially as a function of time, showing the effect of the removal of the acid solutions on hydrogen generation. For steel immersed in H<sub>2</sub>SO<sub>4</sub> solution, the current density, as a function of time, reached values close to zero at approximately 11 h. On the other hand, for steel immersed in HCl, the current density reached a constant value of approximately 1  $\mu\text{A cm}^{-2}$  at 11 h.

The difference between the current densities for steel immersed in the different solutions was associated with the formation of FeSO<sub>4</sub> on the steel, after removal of the H<sub>2</sub>SO<sub>4</sub> solution. Even with the removal of the H<sub>2</sub>SO<sub>4</sub> solution, there was a solution film on the steel. Therefore, the iron ion concentration increased in this solution film. These high iron ion and acid concentrations in the solution film could then favor FeSO<sub>4</sub> formation and block the corrosion reaction on the steel<sup>44</sup>, preventing injection of atomic hydrogen into the steel. On the other hand, removal of the HCl solution could also lead to formation of the solution film, but in this case, there were no solid corrosion products on the steel. Therefore, after removal of the acid solution, the corrosion process could continue to occur. This result was confirmed in the other experiment shown in Figure 5.

Figure 5 shows the  $i_p$  measurements, on the hydrogen detection side, for the SAE 1020 steel during pickling in aqueous HCl solution on the hydrogen generation side. In this experiment, after HCl removal (region 3), the current density decreased as a function of time, until reaching a constant value at approximately 1 h. At 1.25 h, the hydrogen generation side was rinsed three times with deionized water (point 4 in the curve), after which the current density again showed a decreasing trend. The rinsing process resulted in replacement of the HCl solution by deionized water, which decreased the corrosion process and, consequently, also decreased the injection of atomic hydrogen into the steel.

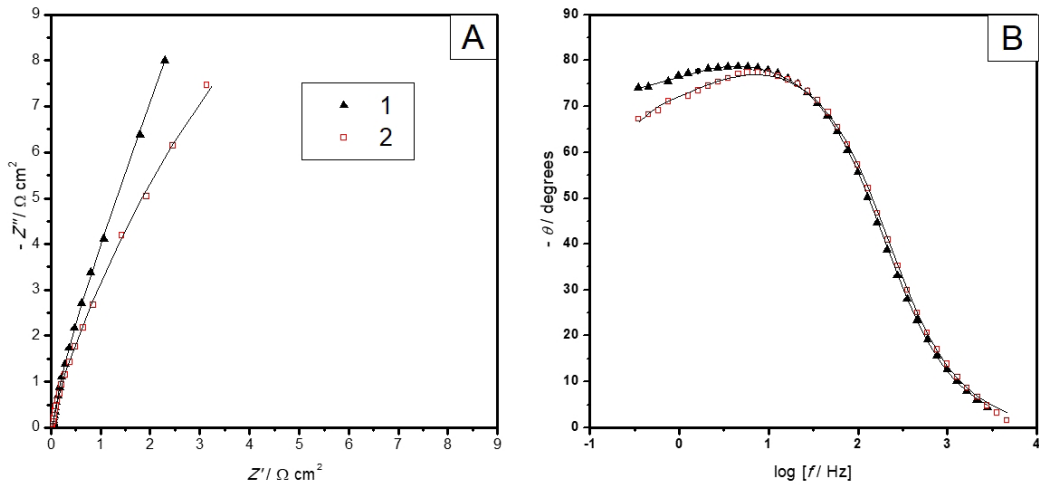


**Figure 6.** Experimental and fitted (continuous lines) complex plane (A) and Bode (B) diagrams obtained for the SAE 1020 steel on the hydrogen detection side, before (1) and during (2) pickling in aqueous HCl solution on the hydrogen detection side.

The oxide film on the hydrogen detection side was also characterized by EIS, before (at 2.25 h) and during hydrogen permeation (at 4 h). Figure 6 shows the complex plane (A) and Bode (B) diagrams obtained with the experimental data, together with the fitted values (continuous lines). The near-vertical form of the plots in the complex plane diagram indicated the dominance of the capacitance associated with the passive oxide films. However, the resistance in this interface was lower during hydrogen permeation than before permeation.

In the Bode diagram, two collapsed time constants were detected, at  $\sim 9.7$  Hz and at a frequency lower than 2.0 Hz, irrespective of the electrolyte used (Figure 6b). However, at lower frequencies, the phase angles were higher without hydrogen permeation than with hydrogen permeation. This indicated that hydrogen permeation decreased the oxide resistivity.

These results suggested that the first time constant, at high frequency, was associated with the double layer capacitance and the charge transfer resistance, while the second time constant, at low frequency, was associated with the oxide film resistance and capacitance.

The EEC shown in Figure 7 was fitted to the experimental data. In this work, the  $n_{ox}$  and  $n_{dl}$  values were within the range  $0.5 < n < 1$  (Table 3), indicative of non-homogeneous current distributions or heterogeneous distributions of the properties of the oxide.

The level of agreement between the fitted and experimental EIS data was evaluated using the chi-square ( $\chi^2$ ) test, with values around  $10^{-3}$  (Table 3) indicating a good fit. To account for non-ideal capacitive responses, the constant phase element (CPE) was employed, with values of the  $n$  parameter falling within the range from 0.5 to 1 (Table 3). This range suggests non-homogeneous current distributions or heterogeneous distributions of the oxide properties<sup>45</sup>.

In this EEC,  $R_s$  corresponds to the electrolyte resistance.  $R_{ct}$  and  $CPE_{dl}$  represent the charge transfer through the double layer nonideal capacitance in the oxide/solution interphase.  $R_{ox}$  and  $CPE_{ox}$  are related to the oxide film (Figure 7). This EEC has also been reported in the literature<sup>46</sup>.

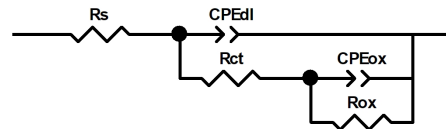


**Figure 7.** Equivalent electrical circuit (EEC) used to fit the impedance data obtained for the SAE 1020 steel on the hydrogen detection side, before and during pickling in aqueous HCl solution on the hydrogen detection side.

The  $Fe_3O_4$  passive film, which has a layered structure formed by the gradient of the  $Fe(III)$  concentration, which increases from the substrate to the solution, has been reported in studies involving the immersion of iron in alkaline solutions. In an  $Fe_3O_4$  passive film without hydrogen permeation, conductivity is attributed to the transport of vacancies through the passive film<sup>46</sup>. However, in an oxide film with hydrogen permeation, the hydrogen atoms partially reduce the oxide layer at the exit side of the metal. As a result, in addition to the transport of vacancies through the passive film, the anodic current recorded with anodic polarization can also be due to a circular mechanism of iron reduction ( $Fe^{2+}$ ) and re-oxidation ( $Fe^{3+}$ )<sup>47</sup>, which decreases the resistance of the oxide film.

The thickness of the passive film prior to hydrogen permeation was obtained using the  $CPE_{ox}$  circuit element, as shown in Figure 7 and Table 2. To establish this, the correlation between  $CPE_{ox}$  and the effective capacitance of the oxide ( $C_{eff}$ ) was determined using Equations 11 and 12<sup>48-50</sup>:

$$C_{eff} = gCPE_{ox} (\rho_0 \epsilon \epsilon_0)^{1-n_{ox}} \quad (11)$$

$$g = 1 + 2.88(1 - n_{ox})^{2.375} \quad (12)$$

where,  $\rho_0$  is the critical interface resistance ( $500 \Omega \text{ cm}^{-1}$ ),  $\epsilon_0$  is the vacuum dielectric constant ( $8.854 \times 10^{-14} \text{ F cm}^{-1}$ )<sup>50</sup>, and  $\epsilon$  is the dielectric constant of the passive film. According to the literature<sup>50</sup>, this value can be considered equal to 12.

The thickness of the oxide passive film can be expressed as follows:

**Table 3.** Equivalent electrical circuit parameter values obtained from fitting of the experimental data. The error % values for each element of the circuit are shown in parentheses.

Conditions	$R_s$ ( $\Omega \text{ cm}^2$ )	$CPE_{dl}^{ox}$ ( $\mu\text{F cm}^{-2} \text{ s}^{\alpha-1}$ )	$n_{dl}$	$R_{ct}$ ( $\text{k}\Omega \text{ cm}^2$ )	$R_{ox}$ ( $\text{k}\Omega \text{ cm}^2$ )	$CPE_{ox}^{ox}$ ( $\mu\text{F cm}^{-2} \text{ s}^{\alpha-1}$ )	$n_{ox}$	$\chi^2$ ( $10^{-3}$ )	$L$ (nm)
Without hydrogen permeation	29 (0.2)	53 (0.6)	0.9 (0.1)	30 (8.7)	48 (30.3)	15 (8.9)	1.0 (11.4)	0.1	69
With hydrogen permeation	28 (0.3)	49 (1.2)	0.9 (0.2)	13 (12.2)	23 (21.9)	22 (9.8)	0.9 (11.9)	0.3	-

$$L = \frac{\epsilon \epsilon_0}{C_{eff}} \quad (13)$$

The calculated thickness of the oxide film was 69 nm (Table 2). Previous work obtained a value of 71.1 nm for the film on Fe-C alloy with 0.7% C, using ellipsometry in 0.05 mol L<sup>-1</sup> KOH, at room temperature<sup>51</sup>.

As shown in Figure 8, the time taken to reach the steady state was approximately 1 h for the 1020 and 1008 steels immersed in HCl solution without any inhibitor, as well as for the 1020 steel in the presence of the inhibitors (EMIM)<sup>+</sup>(Ac)<sup>-</sup> and (EMIM)<sup>+</sup>(Br)<sup>-</sup>. The 1008 steel was only exposed to the (BMIM)<sup>+</sup>(BF<sub>4</sub>)<sup>-</sup> inhibitor, with a longer time taken to achieve the steady state (1.5 h to reach the stationary current). In the presence of HPY, the 1020 steel reached the steady state in 0.5 h and presented the highest  $i_p^{ss}$  values, suggesting that the compound favored hydrogen permeation in the steel.

The different steels presented similar  $i_p$  values in the absence of any inhibitor, even though these steels differ in terms of composition, hardness, and microstructure (Table 1). In previous works<sup>52,53</sup>, it was shown that for 1010 and 1020 steels, the difference between the hydrogen permeability values may be small. Furthermore, in another study<sup>54</sup> was related that the random ferrite/pearlite structure (Table 1) does not affect the hydrogen diffusion and permeability in carbon steel.

The  $i_p^{ss}$  value for the solution without inhibitors, as well as in the presence of HPY, was about 3.2  $\mu\text{A cm}^{-2}$ , while the solutions with (EMIM)<sup>+</sup>(Br)<sup>-</sup>, (EMIM)<sup>+</sup>(Ac)<sup>-</sup>, and (BMIM)<sup>+</sup>(BF<sub>4</sub>)<sup>-</sup> presented  $i_p^{ss}$  values of approximately 2.6, 2.4, and 2.2  $\mu\text{A cm}^{-2}$ , respectively.

To determine the hydrogen permeation inhibition efficiency values, IE<sub>p</sub> (%), Equation 14 was employed<sup>4,28</sup>:

$$IE_p (\%) = 100 \left( \frac{i_p^{ss(o)} - i_p^{ss}}{i_p^{ss(o)}} \right) \quad (14)$$

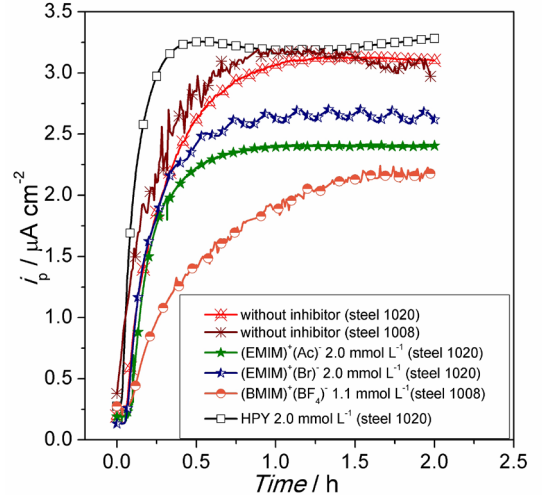
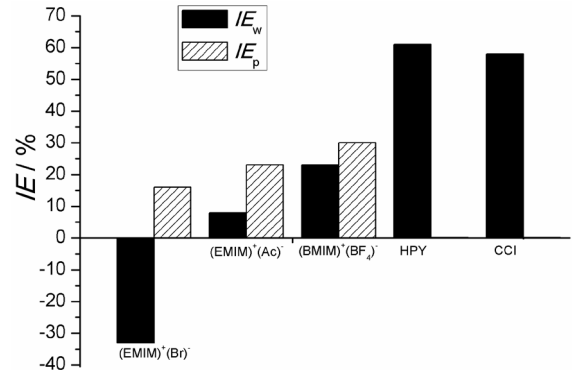
where,  $i_p^{ss(o)}$  and  $i_p^{ss}$  are the steady-state permeation currents in the absence and presence of the inhibitor, respectively.

To calculate the corrosion inhibition efficiency, IE<sub>w</sub> (%), Equation 15 was utilized<sup>55,56</sup>:

$$IE_w (\%) = 100 \left( \frac{w^o - w}{w^o} \right) \quad (15)$$

where,  $w^o$  and  $w$  are the mass loss values in the absence and presence of the inhibitor, respectively.

The addition of (EMIM)<sup>+</sup>(Br)<sup>-</sup> was found to accelerate the corrosion process. However, it also resulted in a 15.8% reduction of hydrogen entry into the steel, as shown in Figure 9.

**Figure 8.** Hydrogen permeation transients for the carbon steels during pickling in aqueous HCl solution, in the absence and presence of (EMIM)<sup>+</sup>(Ac)<sup>-</sup>, (EMIM)<sup>+</sup>(Br)<sup>-</sup>, (BMIM)<sup>+</sup>(BF<sub>4</sub>)<sup>-</sup>, and HPY.**Figure 9.** IE<sub>w</sub> and IE<sub>p</sub> values obtained in the presence of (EMIM)<sup>+</sup>(Ac)<sup>-</sup>, (EMIM)<sup>+</sup>(Br)<sup>-</sup>, (BMIM)<sup>+</sup>(BF<sub>4</sub>)<sup>-</sup>, and HPY.

The increased corrosion could be attributed to the presence of bromide<sup>57</sup>. The large size and ease of polarization of Br<sup>-</sup> lead to lower corrosion inhibition, while smaller anions can interact more easily with the metal surface, leading to stronger adsorption. Furthermore, smaller anions can diffuse more rapidly, leading to better coverage and uniformity of the corrosion inhibitor on the metal surface<sup>58</sup>. The size of the anion can also influence the electrochemical behavior of the IL, affecting parameters such as its redox potential, which can influence the corrosion inhibition mechanism<sup>59-61</sup>.

In these circumstances, the inhibition of hydrogen permeation by  $(EMIM)^+(Br)^-$  was probably not due to blocking by an inhibitor film (geometric blocking), given that the steel presented an accelerated corrosion process. Other possible mechanisms are related to the effects of cations and anions<sup>62,63</sup>. The findings of the present work showed that the anions could influence the entry of hydrogen into the steel (Figure 4). In contrast to the effect of chloride, the permeation of hydrogen increases in the presence of bromide<sup>43</sup>. Since the bromide allowed the entry of hydrogen into the steel and  $(EMIM)^+(Br)^-$  did not protect against corrosion, it is likely that  $(EMIM)^+$  contributed to the inhibition of hydrogen permeation.

In the presence of  $(EMIM)^+(Ac)^-$ , the inhibition process was not effective against corrosion ( $IE_{corr} = 8\%$ ), while there was an approximately 23% reduction of hydrogen entry into the steel (Figure 9). In addition to  $(EMIM)^+$ , the  $(Ac)^-$  counter ion may also affect hydrogen inhibition<sup>64</sup>.

Although the  $(BMIM)^+(BF_4)^-$  concentration was lower than those of  $(EMIM)^+(Ac)^-$  and  $(EMIM)^+(Br)^-$ , this compound provided higher corrosion and hydrogen permeation inhibition efficiency values (23% and 30%, respectively), compared to the other ionic liquids (Figure 9).

Earlier work investigated the effects of quaternary ammonium salt ILs on the absorption of hydrogen by mild steel in hydrochloric acid solution<sup>14</sup>. It was observed that the compounds inhibited steel dissolution and hydrogen absorption, which was attributed to a decrease in the rate constant for discharge of  $H^+$  ions (reaction 6) and an increase of reaction 7.

The optimal corrosion inhibition was achieved with HPY, which exhibited an inhibition efficiency of 61% (as shown in Figure 9). This was probably due to the ability of the inhibitor to obstruct the formation of hydrogen molecules on the surface of the steel. In other words, the HPY compound could adsorb on cathodic sites, preventing hydrogen molecule formation and consequently accelerating the penetration of atomic hydrogen into the steel<sup>16,65</sup>.

The permeation inhibition efficiency of a commercial corrosion inhibitor (CCI) was also evaluated for steel with the presence of scale, during pickling in aqueous HCl solution (Figure 10). The carbon steel obtained after the hot strip mill process presented  $i_p^{ss}$  values smaller than those obtained for the 1008 and 1020 steels.

For the solution without inhibitor, the time required to reach the maximum permeation current was approximately 40 min, compared to a time of around 25 min in the presence of the CCI. The maximum permeation currents were similar for the two solutions. However, after 0.4 h, the permeation current for the solution with the inhibitor decreased as a function of time, from  $2.8 \mu A cm^{-2}$  at 25 min to  $2.4 \mu A cm^{-2}$  at 2 h, indicating that the inhibitor was unable to protect against hydrogen permeation up to 25 min. The corrosion inhibition efficiency was 58% (Figure 9).

### 3.2. Quantum chemical calculations

Quantum chemical calculations based on density functional theory (DFT) were used to study the effect of electronic structure on the corrosion inhibition efficiencies of the compounds HPY and  $(BMIM)^+(BF_4)^-$ . The ionic liquids

$(EMIM)^+(Ac)^-$  and  $(EMIM)^+(Br)^-$  were not included in the calculations, because they did not exhibit efficient inhibition.

The inhibition efficiencies were evaluated using theoretical corrosion inhibition parameters. The results for the calculated quantum chemical parameters are listed in Table 4.

The HOMO energy and the HOMO–LUMO gap ( $\Delta E$ ) are very important for studying the reactivity and stability of structures. According to the literature, the adsorption of the inhibitor on the metal surface increases with increasing HOMO energy<sup>28,36,55</sup>. A high  $E_{HOMO}$  value is associated with a strong tendency to donate electrons into the vacant d orbitals of the metal surface. It can be seen that the  $E_{HOMO}$  values for the inhibitors followed the order  $HPY > (BMIM)^+(BF_4)^-$ .

Another important parameter for evaluation of reactivity is the energy gap between HOMO and LUMO. The calculated results showed that the order of the energy gap was  $HPY < (BMIM)^+(BF_4)^-$ . A smaller energy gap value indicates lower stability, high polarizability, and high chemical reactivity, which is reflected in higher corrosion inhibition efficiency.

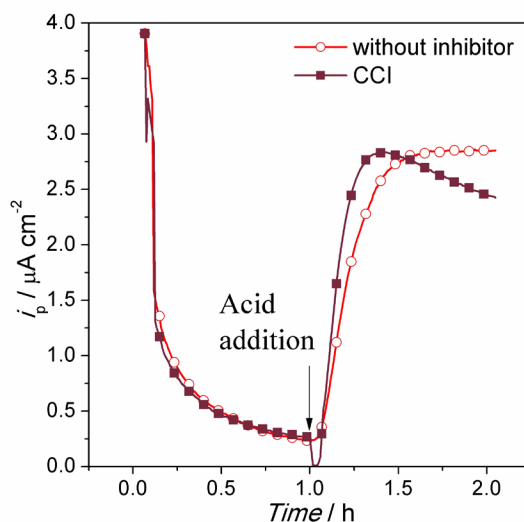


**Figure 10.** Hydrogen permeation transients for the steel with presence of scale, during pickling in aqueous HCl solutions, in the absence and presence of the CCI.

**Table 4.** Quantum chemical parameters of the inhibitors, obtained using density functional theory (B3LYP/6-311G(d,p)).

Parameters	HPY	$(BMIM)^+(BF_4)^-$
$E_{HOMO}$ (eV)	-6.06	-7.69
$E_{LUMO}$ (eV)	-1.28	-0.91
I (eV)	6.06	7.69
A (eV)	1.28	0.91
$\Delta E$ (eV)	4.78	6.78
$\chi$	3.67	4.30
$\eta$ (eV)	2.39	3.39
S ( $eV^{-1}$ )	0.418	0.295
$\Delta N$	0.70	0.40



According to the Pearson HSAB principle, a hard molecule is associated with low basicity and low electron donating ability, while a soft molecule is associated with high basicity and high electron donating tendency<sup>66,67</sup>. In this study, the values of global hardness and softness followed the order  $\text{HPY} > (\text{BMIM})^+(\text{BF}_4)^-$ .

The literature reports that a positive number for the fraction of transferred electrons indicates that the molecule acts as an electron acceptor. In the present work, all the  $\Delta N$  values were positive, indicating that all the inhibitors were able to donate electrons to the metal surface<sup>68</sup>.

Quantum chemical parameters such as the HOMO energy, the energy gap ( $\Delta E$ ), global hardness ( $\eta$ ), and chemical softness are crucial properties of a reactive inhibitor molecule for adsorption on the metal surface. An efficient inhibitor is characterized by a small energy gap. Therefore, it can be seen from the values in Table 3 that HPY was the better inhibitor. The low energy gap could be attributed to relative destabilization of the HOMO or stabilization of the LUMO.

The highest occupied molecular orbital (HOMO), lowest unoccupied molecular orbital (LUMO), and electrostatic potential (ESP) for the inhibitors are shown in Figure 11.

In Figure 11, negative electrostatic potential regions (red) are favorable for electrophilic attack. On the other hand, positive electrostatic potential regions (blue) are favorable for nucleophilic attack.

The HOMO and LUMO surfaces of the HPY inhibitor showed the  $\pi$  and  $\pi^*$  character of hexahydropyrimidine moieties. On the other hand, the HOMO of  $(\text{BMIM})^+(\text{BF}_4)^-$  was distributed over the anion units and showed a typical  $\sigma$  bond. The LUMO surface of  $(\text{BMIM})^+(\text{BF}_4)^-$  contained contributions from the imidazolium ring.

Therefore, for the compounds studied here, the inhibition efficiency was in the following order:  $\text{HPY} > (\text{BMIM})^+(\text{BF}_4)^-$ .

### 3.3. *In silico* toxicity evaluation

Considering the need for corrosion inhibitors that are both efficient and environmentally friendly, it was important to evaluate the toxicity of HPY, since traditional inorganic and organic inhibitors tend to be toxic and polluting<sup>69</sup>. *In silico* tools have limitations, but they are easy to use, inexpensive, and allow the assessment of toxicity when no experimental information is available.

T.E.S.T. mutagenicity evaluations were obtained using the hierarchical clustering method<sup>38</sup>. This method was chosen because it provided the best matches between predicted and experimental values for similar chemicals in the training set. The prediction showed that HPY should be non-mutagenic.

The Toxtree results agreed with the T.E.S.T. predictions, also indicating that HPY has no potential mutagenicity.

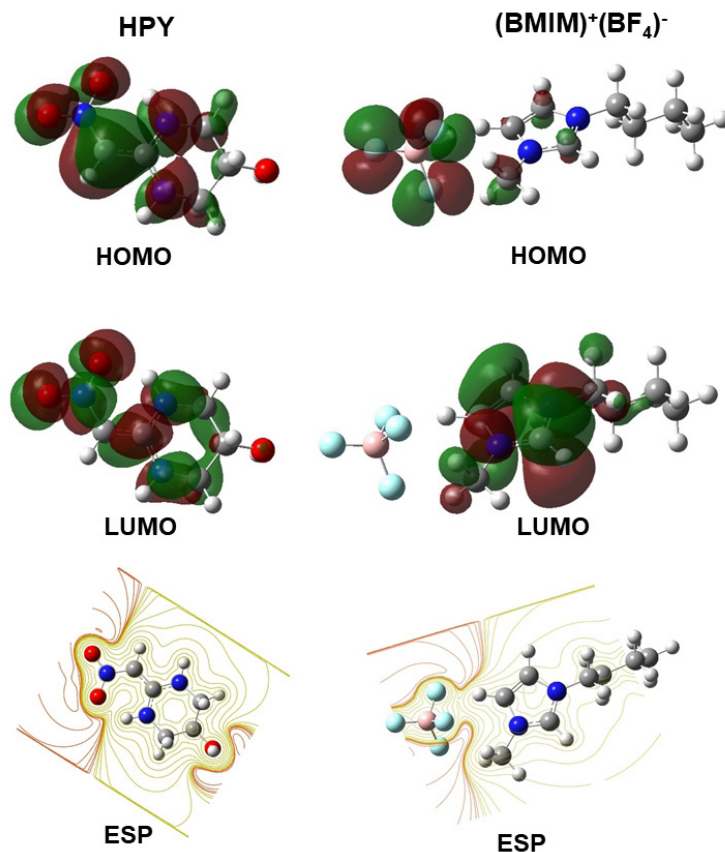


**Figure 11.** Frontier molecular orbital surfaces (HOMO and LUMO) and ESP for the inhibitors (a) HPY and (b)  $(\text{BMIM})^+(\text{BF}_4)^-$ .

Toxtree also predicted that the compound has no potential carcinogenicity.

Although ILs used to be low toxicity, many of them now present moderate to very high toxicity. For example, (BMIM)<sup>+</sup>(BF<sub>4</sub>)<sup>-</sup> has been shown to be effective in inhibiting corrosion and hydrogen permeation, but it has a moderate toxicity level<sup>70</sup>. This highlights the importance of performing previous *in silico* evaluation, before synthesizing and testing new compounds, in order to save time and resources in the search for green corrosion inhibitors.

Finally, our research group has been trying to discover a method to produce an inhibitor that combines the characteristics of HPY and (BMIM)<sup>+</sup>(BF<sub>4</sub>)<sup>-</sup>. For this, it is necessary to alkylate the nitrogens of the cyclic system. However, it is not known whether the nitrogens are rich in electrons, due to resonance with the nitro methylene group, or whether the alkylation will not harm the inhibition. Therefore, further theoretical and experimental investigations are needed.

## 4. Conclusions

The pickling process in 5.4 mol L<sup>-1</sup> HCl solution decreased the hydrogen permeation current by 50%, although there was no difference between the rates of corrosion of steel in HCl and H<sub>2</sub>SO<sub>4</sub> (2.7 mol L<sup>-1</sup>). The resistance of the passive film on the detection side decreased during the permeation of hydrogen.

The different steels presented similar  $i_p$  values in the absence of any inhibitor, even though these steels have different compositions and microstructures. The carbon steel obtained after the hot strip mill process presented  $i_p^{ss}$  values smaller than those obtained for the 1008 and 1020 steels.

The cations and anions of ILs play important roles in the inhibition of hydrogen permeation in carbon steel. The compound (BMIM)<sup>+</sup>(BF<sub>4</sub>)<sup>-</sup> presented efficiencies of 23% and 30% for the prevention of corrosion and entry of hydrogen into the steel, respectively. The compounds (EMIM)<sup>+</sup>(Br)<sup>-</sup> and (EMIM)<sup>+</sup>(Ac)<sup>-</sup> were not effective against corrosion, possibly due to the high HCl concentration and the low inhibitor concentration (2 mmol L<sup>-1</sup>), but presented efficiencies of 15.8% and 23%, respectively, for reduction of hydrogen entry into the steel.

The compound HPY provided more effective corrosion inhibition (61%). In contrast, this compound and the CCI did not inhibit hydrogen permeation.

Although it was not possible to predict the inhibition of hydrogen permeation, the results obtained using DFT (B3LYP/6-311G(d,p)) for (BMIM)<sup>+</sup>(BF<sub>4</sub>)<sup>-</sup> and HPY revealed that the quantum chemical parameters and inhibitor efficiency were closely related. The theoretical quantum study demonstrated that the inhibition efficiency increased with increase of  $E_{\text{HOMO}}$  and decreases of  $E_{\text{LUMO}}$  and the energy gap ( $\Delta E$ ). The order of corrosion inhibition found by the theoretical calculation, HPY > (BMIM)<sup>+</sup>(BF<sub>4</sub>)<sup>-</sup>, agreed with the inhibition efficiencies observed experimentally.

Combining these conclusions with *in silico* toxicity predictions, it will be possible to propose new compounds as potential nontoxic corrosion inhibitor candidates, for further synthesis and electrochemical evaluation.

## 5. Acknowledgments

The authors thank the Brazilian funding agencies Fomento à Pesquisa na Universidade Federal Fluminense (FOPESQ-2020/2021/2022 financial support programs), Programa Institucional de Bolsas de Iniciação Científica (PIBIC/UFF-2021/2022), Conselho Nacional de Desenvolvimento Científico e Tecnológico (CNPq grant Produtividade em Pesquisa-PQ 2/Processo: 309873/2022-3), and Fundação de Amparo à Pesquisa do Estado do Rio de Janeiro (FAPERJ grants E-26/010.101125/2018 and E-26/010.002199/2019). The authors thanks also the Campanha Siderúrgica Nacional (CSN) for steels microstructure characterization. This study was also financed in part by Coordenação de Aperfeiçoamento de Pessoal de Nível Superior - Brasil (CAPES, Finance Code 001).

## 6. References

- Hudson RM. Hydrogen absorption by and dissolution rate of low-carbon steel in sulfuric, hydrochloric, phosphoric and nitric acids. *Corrosion*. 1964;20(8):245-51t. <http://dx.doi.org/10.5006/0010-9312-20.8.245t>.
- Sastri VS. Corrosion inhibitors: other important applications. In: Cottis B, Graham M, Lindsay R, Lyon S, Richardson T, Scantlebury D, et al., editors. *Shreir's corrosion*. Amsterdam: Elsevier; 2010. Chapter 4.29; p. 2990-3000. <http://dx.doi.org/10.1016/B978-0-44452787-5.00163-3>.
- Silva AN, Costa EC, Almeida JG, Maciel TM, Cavalcante DGL, Passos TA. Effect of hydrogen on the mechanical properties of ASTM A182 F22 and ASTM A36 steels welded joint using Inconel 625 as filler and buttering metal. *Mater Res*. 2022;25:e20210339. <http://dx.doi.org/10.1590/1980-5373-mr-2021-0339>.
- Ramesh Babu B, Holze R. Corrosion and hydrogen permeation inhibition for mild steel in HCl by isomers of organic compounds. *Br Corros J*. 2000;35(3):204-9. <http://dx.doi.org/10.1179/000705900101501254>.
- Yu S-H, Lyu A, Jang I-S, Park HS, Jang M, Lee KY, et al. Hydrogen absorption, desorption and embrittlement of Zn and ZnNi-electrodeposited bolts. *J Mater Res Technol*. 2021;11:1604-10. <http://dx.doi.org/10.1016/j.jmrt.2021.02.006>.
- Aromaa J, Pehkonen A, Schmachtel S, Galfi I, Forsén O. Electrochemical determination of hydrogen entry to HSLA steel during pickling. *Adv Mater Sci Eng*. 2018;2018:1-7. <http://dx.doi.org/10.1155/2018/3676598>.
- Kuklík V, Kudláček J. Hot-dip galvanizing of steel structures. Oxford: Elsevier; 2016. Chapter 13, Hot-dip galvanizing and the environment; p. 199-202. <http://dx.doi.org/10.1016/B978-0-08-100753-2.00013-6>.
- Ituen EB, Solomon MM, Umoren SA, Akaranta O. Corrosion inhibition by amitriptyline and amitriptyline based formulations for steels in simulated pickling and acidizing media. *J Petrol Sci Eng*. 2019;174:984-96. <http://dx.doi.org/10.1016/j.petrol.2018.12.011>.
- Alaoui Mouayd A, Orazem ME, Sutter EMM, Tribollet B, Koltsov A. Contribution of electrochemical dissolution during pickling of low carbon steel in acidic solutions. *Corros Sci*. 2014;82:362-8. <http://dx.doi.org/10.1016/j.corsci.2014.01.036>.
- Umoren SA, Solomon MM, Obot IB, Suleiman RK. A critical review on the recent studies on plant biomaterials as corrosion inhibitors for industrial metals. *J Ind Eng Chem*. 2019;76:91-115. <http://dx.doi.org/10.1016/j.jiec.2019.03.057>.
- Amokrane N, Gabrielli C, Maurin G, Mirkova L. Effect of organic additives on hydrogen permeation into an iron membrane

- studied by frequency analysis techniques. *Electrochim Acta*. 2007;53(4):1962-71. <http://dx.doi.org/10.1016/j.electacta.2007.08.053>.
12. Finšgar M, Jackson J. Application of corrosion inhibitors for steels in acidic media for the oil and gas industry: a review. *Corros Sci*. 2014;86:17-41. <http://dx.doi.org/10.1016/j.corsci.2014.04.044>.
  13. Rengamani S, Muralidharan S, Anbu Kulandainathan M, Venkatakrishna Iyer S. Inhibiting and accelerating effects of aminophenols on the corrosion and permeation of hydrogen through mild steel in acidic solutions. *J Appl Electrochem*. 1994;24(4). <http://dx.doi.org/10.1007/BF00242066>.
  14. Avdeev YG, Nenasheva TA, Luchkin AY, Marshakov AI, Kuznetsov YI. Effect of quaternary ammonium salts and 1,2,4-triazole derivatives on hydrogen absorption by mild steel in hydrochloric acid solution. *Materials*. 2022;15(19):6989. <http://dx.doi.org/10.3390/ma15196989>.
  15. Naveen E, Ramnath BV, Elanchezhian C, Nazirudeen SSM. Influence of organic corrosion inhibitors on pickling corrosion behaviour of sinter-forged C45 steel and 2% Cu alloyed C45 steel. *J Alloys Compd*. 2017;695:3299-309. <http://dx.doi.org/10.1016/j.jallcom.2016.11.133>.
  16. Dwivedi D, Lepková K, Becker T. Carbon steel corrosion: a review of key surface properties and characterization methods. *RSC Advances*. 2017;7(8):4580-610. <http://dx.doi.org/10.1039/C6RA25094G>.
  17. Silva MG, Araujo RG, Silvério RL, Costa ANC, Sangi DP, Pedrosa LF, et al. Inhibition effects of ionic and non-ionic derivatives of imidazole compounds on hydrogen permeation during carbon steel pickling. *J Mater Res Technol*. 2022;16:1324-38. <http://dx.doi.org/10.1016/j.jmrt.2021.12.068>.
  18. Corrales-Luna M, Le Manh T, Romero-Romo M, Palomar-Pardavé M, Arce-Estrada EM. 1-Ethyl 3-methylimidazolium thiocyanate ionic liquid as corrosion inhibitor of API 5L X52 steel in H<sub>2</sub>SO<sub>4</sub> and HCl media. *Corros Sci*. 2019;153:85-99. <http://dx.doi.org/10.1016/j.corsci.2019.03.041>.
  19. Jeon Y, Sung J, Seo C, Lim H, Cheong H, Kang M, et al. Structures of ionic liquids with different anions studied by infrared vibration spectroscopy. *J Phys Chem B*. 2008;112(15):4735-40. <http://dx.doi.org/10.1021/jp7120752>.
  20. Qiang Y, Zhang S, Yan S, Zou X, Chen S. Three indazole derivatives as corrosion inhibitors of copper in a neutral chloride solution. *Corros Sci*. 2017;126:295-304. <http://dx.doi.org/10.1016/j.corsci.2017.07.012>.
  21. Yesudass S, Olasunkanmi LO, Bahadur I, Kabanda MM, Obot IB, Ebenso EE. Experimental and theoretical studies on some selected ionic liquids with different cations/anions as corrosion inhibitors for mild steel in acidic medium. *J Taiwan Inst Chem Eng*. 2016;64:252-68. <http://dx.doi.org/10.1016/j.jtice.2016.04.006>.
  22. Verma C, Olasunkanmi LO, Bahadur I, Lgaz H, Quraishi MA, Haque J, et al. Experimental, density functional theory and molecular dynamics supported adsorption behavior of environmental benign imidazolium based ionic liquids on mild steel surface in acidic medium. *J Mol Liq*. 2019;273:1-15. <http://dx.doi.org/10.1016/j.molliq.2018.09.139>.
  23. Yousefi A, Javadian S, Dalir N, Kakemam J, Akbari J. Imidazolium-based ionic liquids as modulators of corrosion inhibition of SDS on mild steel in hydrochloric acid solutions: experimental and theoretical studies. *RSC Advances*. 2015;5(16):11697-713. <http://dx.doi.org/10.1039/C4RA10995C>.
  24. Xu Y, Huang Y, Cai F, Wang Z, Lu D, Wang X, et al. Evaluation of hydrogen permeation into high-strength steel during corrosion in different marine corrosion zones. *Appl Sci*. 2022;12(6):2785. <http://dx.doi.org/10.3390/app12062785>.
  25. Abdulazeez I, Al-Hamouz OCS, Khaled M, Al-Saadi AA. Inhibition of mild steel corrosion in CO<sub>2</sub> and H<sub>2</sub>S-saturated acidic media by a new polyurea-based material. *Mater Corros*. 2020;71(4):646-62. <http://dx.doi.org/10.1002/maco.201911270>.
  26. Boudjellal F, Ouici HB, Guendouzi A, Benali O, Sehmi A. Experimental and theoretical approach to the corrosion inhibition of mild steel in acid medium by a newly synthesized pyrazole carbothioamide heterocycle. *J Mol Struct*. 2020;1199:127051. <http://dx.doi.org/10.1016/j.molstruc.2019.127051>.
  27. Oukhrib R, Abdellaoui Y, Berisha A, Abou Oualid H, Halili J, Jusufi K, et al. DFT, Monte Carlo and molecular dynamics simulations for the prediction of corrosion inhibition efficiency of novel pyrazolylnucleosides on Cu(111) surface in acidic media. *Sci Rep*. 2021;11(1):3771. <http://dx.doi.org/10.1038/s41598-021-82927-5>.
  28. Silva MG, Araujo RG, Silvério RL, Costa ANC, Sangi DP, Pedrosa LF, et al. Inhibition effects of ionic and non-ionic derivatives of imidazole compounds on hydrogen permeation during carbon steel pickling. *J Mater Res Technol*. 2022;16:1324-38. <http://dx.doi.org/10.1016/j.jmrt.2021.12.068>.
  29. Obot IB, Macdonald DD, Gasem ZM. Density functional theory (DFT) as a powerful tool for designing new organic corrosion inhibitors. Part 1: an overview. *Corros Sci*. 2015;99:1-30. <http://dx.doi.org/10.1016/j.corsci.2015.01.037>.
  30. Fathabadi HE, Ghorbani M, Ghartavol HM. Corrosion inhibition of mild steel with tolyltriazole. *Mater Res*. 2021;24(4):e20200395. <http://dx.doi.org/10.1590/1980-5373-mr-2020-0395>.
  31. Foks H, Pancechowska-Ksepko D, Janowiec M, Zwolska Z, Augustynowicz-Kopeć E. Synthesis and tuberculostatic activity of some 1,1-bis-methylthio-2-nitro-ethene derivatives. *Phosphorus Sulfur Silicon Relat Elem*. 2005;180(10):2291-7. <http://dx.doi.org/10.1080/104265090920921>.
  32. Nardeli JV, Fugivara CS, Benedetti AV. Assessment of charge transport through barrier membranes before application on materials surfaces. *Mater Res*. 2022;25:e20220129. <http://dx.doi.org/10.1590/1980-5373-mr-2022-0129>.
  33. Becke AD. Density-functional exchange-energy approximation with correct asymptotic behavior. *Phys Rev A Gen Phys*. 1988;38(6):3098-100. <http://dx.doi.org/10.1103/PhysRevA.38.3098>.
  34. Becke AD. Density-functional thermochemistry. III. The role of exact exchange. *J Chem Phys*. 1993;98(7):5648-52. <http://dx.doi.org/10.1063/1.464913>.
  35. Frisch MJ, Trucks GW, Schlegel HB, Scuseria GE, Robb MA, Cheeseman JR, et al. *Gaussian 09w*. Wallingford: Gaussian, Inc.; 2009.
  36. Obot IB, Macdonald DD, Gasem ZM. Density functional theory (DFT) as a powerful tool for designing new organic corrosion inhibitors. Part 1: an overview. *Corros Sci*. 2015;99:1-30. <http://dx.doi.org/10.1016/j.corsci.2015.01.037>.
  37. Koopmans T. Über die zuordnung von wellenfunktionen und eigenwerten zu den einzelnen elektronen eines atoms. *Physica*. 1934;1(1-6):104-13. [http://dx.doi.org/10.1016/S0031-8914\(34\)90011-2](http://dx.doi.org/10.1016/S0031-8914(34)90011-2).
  38. Martin T. User's guide for T.E.S.T. version 4.2 (Toxicity Estimation Software Tool): a program to estimate toxicity from molecular structure. Washington, DC: U.S. EPA Office of Research and Development; 2016.
  39. Patlewicz G, Jeliakova N, Safford RJ, Worth AP, Aleksiev B. An evaluation of the implementation of the Cramer classification scheme in the Toxtree software. *SAR QSAR Environ Res*. 2008;19(5-6):495-524. <http://dx.doi.org/10.1080/10629360802083871>.
  40. Benigni R, Bossa C, Tcheremenskaia O. Nongenotoxic carcinogenicity of chemicals: mechanisms of action and early recognition through a new set of structural alerts. *Chem Rev*. 2013;113(5):2940-57. <http://dx.doi.org/10.1021/cr300206t>.
  41. Dafft EG, Bohnenkamp K, Engell HJ. Investigations of the hydrogen evolution kinetics and hydrogen absorption by iron electrodes during cathodic polarization. *Corros Sci*. 1979;19(7):591-612. [http://dx.doi.org/10.1016/S0010-938X\(79\)80061-X](http://dx.doi.org/10.1016/S0010-938X(79)80061-X).
  42. Fraenkel D. Structure and ionization of sulfuric acid in water. *New J Chem*. 2015;39(7):5124-36. <http://dx.doi.org/10.1039/C5NJ00167F>.
  43. Allam AM, Ateya BG, Pickering HW. Effect of chloride ions on adsorption and permeation of hydrogen in iron. *Corrosion*. 1997;53(4):284-9. <http://dx.doi.org/10.5006/1.3280469>.

44. Ellison BT, Schmeal WR. Corrosion of steel in concentrated sulfuric acid. *J Electrochem Soc.* 1978;125(4):524-31. <http://dx.doi.org/10.1149/1.2131491>.
45. Barsoukov E, MacDonald JR, editors. *Impedance spectroscopy: theory, experiment, and applications.* Hoboken: Wiley; 2005. <http://dx.doi.org/10.1002/0471716243>.
46. Sánchez M, Gregori J, Alonso C, García-Jareño JJ, Takenouti H, Vicente F. Electrochemical impedance spectroscopy for studying passive layers on steel rebars immersed in alkaline solutions simulating concrete pores. *Electrochim Acta.* 2007;52(27):7634-41. <http://dx.doi.org/10.1016/j.electacta.2007.02.012>.
47. Vecchi L, Simillion H, Montoya R, Van Laethem D, Van den Eckhout E, Verbeken K, et al. Modelling of hydrogen permeation experiments in iron alloys: characterization of the accessible parameters. Part I: the entry side. *Electrochim Acta.* 2018;262:57-65. <http://dx.doi.org/10.1016/j.electacta.2017.12.172>.
48. Mohammadi M, Choudhary L, Gadala IM, Alfantazi A. Electrochemical and passive layer characterizations of 304L, 316L, and Duplex 2205 stainless steels in thiosulfate gold leaching solutions. *J Electrochem Soc.* 2016;163(14):C883-94. <http://dx.doi.org/10.1149/2.0841614jes>.
49. Hirschorn B, Orazem ME, Tribollet B, Vivier V, Frateur I, Musiani M. Constant-phase-element behavior caused by resistivity distributions in films. *J Electrochem Soc.* 2010;157(12):C452. <http://dx.doi.org/10.1149/1.3499564>.
50. Du W, Liu C, Yue Y. Effect of passivation on the high-temperature oxidation behavior of hot-formed steel. *Corros Sci.* 2022;202:110318. <http://dx.doi.org/10.1016/j.corsci.2022.110318>.
51. Flis J, Oranowska H, Szklarska-Smialowska Z. An ellipsometric study of surface films grown on iron and iron-carbon alloys in 0.05 M KOH. *Corros Sci.* 1990;30(11):1085-99. [http://dx.doi.org/10.1016/0010-938X\(90\)90058-D](http://dx.doi.org/10.1016/0010-938X(90)90058-D).
52. Gadgeel VL, Johnson DL. Gas-phase hydrogen permeation and diffusion in carbon steels as a function of carbon content from 500 to 900 K. *J Mater Energy Syst.* 1979;1(2):32-40. <http://dx.doi.org/10.1007/BF02833976>.
53. Johnson DL, Wu JK. Hydrogen transport in carbon steels as a function of carbon content and heat treatment near 298 K. *J Mater Energy Syst.* 1987;8(4):402-8. <http://dx.doi.org/10.1007/BF02833488>.
54. Tau L, Chan SLI. Effects of ferrite/pearlite alignment on the hydrogen permeation in a AISI 4130 steel. *Mater Lett.* 1996;29(1-3):143-7. [http://dx.doi.org/10.1016/S0167-577X\(96\)00140-1](http://dx.doi.org/10.1016/S0167-577X(96)00140-1).
55. Silva MG, Costa ANC, Sangi DP, Yoned J, Coelho LW, Ferreira EA. Comparative study of oxazolidine and imidazolidine compounds as inhibitors of SAE 1020 steel corrosion in aqueous HCl solution. *Chem Eng Commun.* 2022;209(9):1165-81. <http://dx.doi.org/10.1080/00986445.2021.1940154>.
56. Sánchez-Elleuterio A, Mendoza-Merlos C, Corona Sánchez R, Navarrete-López AM, Martínez Jiménez A, Ramírez-Domínguez E, et al. Experimental and theoretical studies on acid corrosion inhibition of API 5L X70 steel with novel 1-N- $\alpha$ -d-glucopyranosyl-1H-1,2,3-triazole xanthenes. *Molecules.* 2023;28(1):460. <http://dx.doi.org/10.3390/molecules28010460>.
57. Nahlé AH, Harvey TJ, Walsh FC. Quaternary aryl phosphonium salts as corrosion inhibitors for iron in HCl. *J Alloys Compd.* 2018;765:812-25. <http://dx.doi.org/10.1016/j.jallcom.2018.06.241>.
58. Hackerman N, Snavely ES, Payne JS. Effects of anions on corrosion inhibition by organic compounds. *J Electrochem Soc.* 1966;113(7):677. <http://dx.doi.org/10.1149/1.2424089>.
59. Cornejo Robles E, Olivares-Xometl O, Likhanova NV, Arellanes-Lozada P, Lijanova IV, Díaz-Jiménez V. Synthesis of ammonium-based ILs with different lengths of aliphatic chains and organic halogen-free anions as corrosion inhibitors of API X52 steel. *Int J Mol Sci.* 2023;24(8):7613. <http://dx.doi.org/10.3390/ijms24087613>.
60. Al-Rashed O, Abdel Nazeer A. Effectiveness of some novel ionic liquids on mild steel corrosion protection in acidic environment: experimental and theoretical inspections. *Materials.* 2022;15(6):2326. <http://dx.doi.org/10.3390/ma15062326>.
61. Tian G, Yuan K. Performance and mechanism of alkylimidazolium ionic liquids as corrosion inhibitors for copper in sulfuric acid solution. *Molecules.* 2021;26(16):4910. <http://dx.doi.org/10.3390/molecules26164910>.
62. Bockris JO, McBreen J, Nanis L. The hydrogen evolution kinetics and hydrogen entry into  $\alpha$ -iron. *J Electrochem Soc.* 1965;112(10):1025. <http://dx.doi.org/10.1149/1.2423335>.
63. Kimura M, Totsuka N, Kurisu T, Hane T, Nakai Y. Effect of environmental factors on hydrogen permeation in line pipe steel. *Corrosion.* 1988;44(10):738-44. <http://dx.doi.org/10.5006/1.3584939>.
64. Sundararajan T, Akiyama E, Tsuzaki K. Acetate and chloride effects on hydrogen production across crevices. *Mater Sci Forum.* 2006;512:97-102. <http://dx.doi.org/10.4028/www.scientific.net/MSF.512.97>.
65. Marcus P. *Corrosion mechanisms in theory and practice (corrosion technology).* 2nd ed. New York: Marcel Dekker; 2002. <http://dx.doi.org/10.1201/9780203909188>.
66. Pearson RG. Recent advances in the concept of hard and soft acids and bases. *J Chem Educ.* 1987;64(7):561. <http://dx.doi.org/10.1021/ed064p561>.
67. Pearson RG. Hard and soft acids and bases. *J Am Chem Soc.* 1963;85(22):3533-9. <http://dx.doi.org/10.1021/ja00905a001>.
68. Erdoğan Ş, Safi ZS, Kaya S, Işın DÖ, Guo L, Kaya C. A computational study on corrosion inhibition performances of novel quinoline derivatives against the corrosion of iron. *J Mol Struct.* 2017;1134:751-61. <http://dx.doi.org/10.1016/j.molstruc.2017.01.037>.
69. Zhang Q, Zhang R, Wu R, Luo Y, Guo L, He Z. Green and high-efficiency corrosion inhibitors for metals: a review. *J Adhes Sci Technol.* 2022;37(9):1501-24. <http://dx.doi.org/10.1080/01694243.2022.2082746>.
70. Fatemi MH, Izadiyan P. Cytotoxicity estimation of ionic liquids based on their effective structural features. *Chemosphere.* 2011;84(5):553-63. <http://dx.doi.org/10.1016/j.chemosphere.2011.04.021>.